PROCEEDINGS OF SCIENCE

Results of a new approach to the analysis of multi-wavelength observations data obtained with RATAN-600

N. E. Ovchinnikova,* **M. K. Lebedev, V. M. Bogod, A. M. Ripak and A. A. Storozhenko**

Special Astrophysical Observatory of RAS,
Nizhny Arkhyz, Russia
E-mail: n.e.ovchinnikova@gmail.com, m.k.lebedev@gmail.com, vbog_spb@mail.ru, anatoly.ripak@gmail.com, acs-work@mail.ru

Data from solar observations with the RATAN-600 radio telescope in the 1–3 GHz and 3–18 GHz ranges were processed using multivariate statistical methods. This kind of analysis allows us to differentiate the radio sources in the active regions (ARs) on the Sun by their individual flux spectra and trace their evolution during the entire time they have been in sight, as well as to reveal fast processes in a narrow spectral range or in certain areas. It was found that we can isolate twisted magnetic loops in flare-productive ARs in our data, and detect gyrosynchrotron radio emission caused by the non-thermal electrons inside them. Also, we detected an absorption line close to 1.6 GHz with a variable frequency shift in several AR. It may be attributed to the hydroxyl in cool coronal mass, such as solar prominences and coronal rain.

The Multifaceted Universe: Theory and Observations - 2022 (MUTO2022)
23-27 May 2022
SAO RAS, Nizhny Arkhyz, Russia

*Speaker

PoS(MUTO2022)007

Introduction

A new *digital spectropolarimetric complex with RFI excision* provides solar observations in the decimeter wavelength range with the RATAN-600 in the 1–3 GHz range with a frequency resolution of 0.12–10 MHz and a time resolution of ~10 ms. Methods of RFI excision exploiting the analysis of statistical properties of the spectra of received noise signals are based on the assumption that astrophysical signals of natural origin have Gaussian statistics, while non-Gaussian artificial interference would introduce certain distortion into the statistical properties of the signal. For the primary RFI excision, a method based on the assessment of the fourth moment of the distribution of signal power values (kurtosis) is used (see our paper "Digital methods of RFI mitigation in radio astronomy" in these proceedings). Nevertheless, some artificial signals have Gaussian statistics. In addition, the large volume of output data makes it difficult to process and visualize them. We applied principal component analysis (PCA) as a first stage of data processing to reduce a complex data set to a lower dimension without loss of information and to filter out the remaining interference and detect the spectral features. PCA optimizes the covariance matrix of the data array, i.e. the representation of the second moment (variance) of the distribution. The directions of maximum data change are consistently selected in the data space: each next line maximizes the residual variation, etc. Thus, the components are uncorrelated, and form an orthogonal basis. With respect to solar radio emission, since the components are sorted by their contribution to total energy, all natural spectral structures are represented by the first few main components. Hence, we get noise, interference and all the localized spectral features with low dispersion as individual components.

The data series from the primary spectropolarimetric *Solar complex* (3–18 GHz) observations with the RATAN-600 coupled with parallel factor (PARAFAC) modeling [1–3] have been used in the diagnosis of the solar radio emission in the centimeter wavelength range. The Solar complex has a frequency resolution of 150 MHz and a time resolution of ~0.2 s.

We have moved on to data calibration by spectral flux density based on the so-called "quiet Sun" (QS) flux spectra, that is, the radio emission flux spectra of the Sun in the regular period of least activity (Solar minimum). We use data from Nobeyama Radio Polarimeters (NoRP) and Radio Solar Telescope Network (RSTN), and data of the microwave brightness temperature spectrum of the quiet Sun [4] to calculate the fraction of the QS spectral flux density received by the RATAN-600 "South + Flat" antenna system beam. The beam patterns (BP) of the RATAN-600 "South + Flat" antenna system where calculated using the aperture field integration method. Then we assume these theoretical values to be the spectra of the first component in the PCA decomposition, or the spectra of the main radio source in the PARAFAC decomposition.

As there is a strong dependence of the BP on wavelength, the spatial resolution of the antenna system changes twofold within the 1–3 GHz frequency range. Thus, we also had to reconstruct the data using least square deconvolution with the theoretical horizontal BP of the RATAN-600 "South + Flat" antenna system at each wavelength.

1. Solar radio emission in 1-3 GHz observations with RATAN-600

The spectral component of the absorption band close to 1.6 GHz was found in the radio emission of certain flare-productive ARs even in the first observations in December of 2021. The

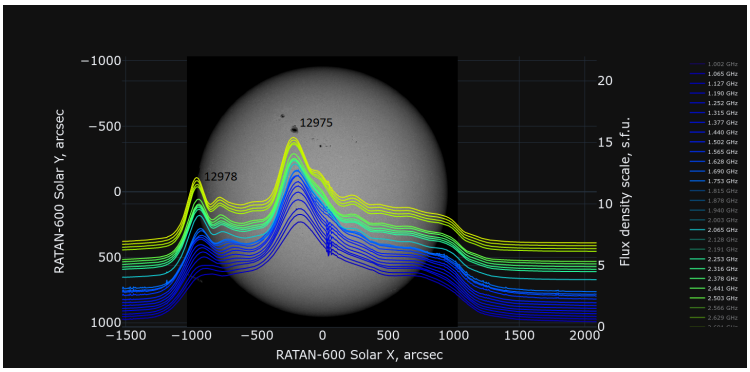

Figure 1: Solar radio emission on 2022.03.27 09:03:00 UTC (1–3 GHz)

FWHM of the band varies from 80 to 150 MHz and the absorption minimum shifts within several tens of MHz. We propose that it may belong to the hyperfine transition frequencies for OH radical in the $v = 0$, $X^2\Pi_{3/2}$ ground state in combined electric and magnetic fields [5]. The most interesting observation was made on March 27, 2022, at 09:03:00 UTC. Fig. 1 shows the calibrated scans of the Sun before deconvolution in the entire 1–3 GHz range together with the HMI magnetogram, rotated to match the RATAN-600 positional angle.

The calibrated data in the spectral range of 1.4–1.8 GHz, reconstructed without a QS component before deconvolution, are presented in Fig. 2 over-plotted on the UV AIA image (171 Å), rotated to match the RATAN-600 positional angle. The minima of the absorption bands above AR NOAA 2978 (on the limb) and AR NOAA 2975 apparently shift along the loops in contrast to the radio emission maxima.

The resulting spectrogram, deconvolved with horizontal BP, is shown in Fig. 3. The area from −880 to −1100 arcsec from the Sun center corresponds to AR NOAA 2978, and the area from −100 to −500 arcsec from the Sun center—to AR NOAA 2975. The intensity is given in arbitrary units. The structure of the absorption band found above AR NOAA 2978 at −880 arcsec from the Sun center corresponds exactly to the hyperfine transition frequencies for OH ground state (1612,

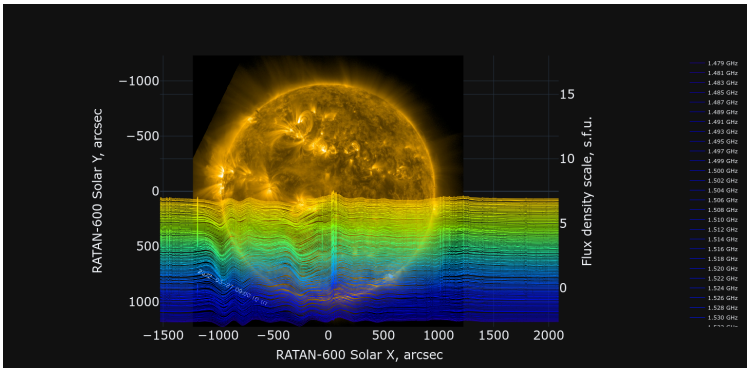

Figure 2: Solar radio emission on 2022.03.27 09:03:00 UTC (1.4–1.8 GHz), reconstructed without the QS component

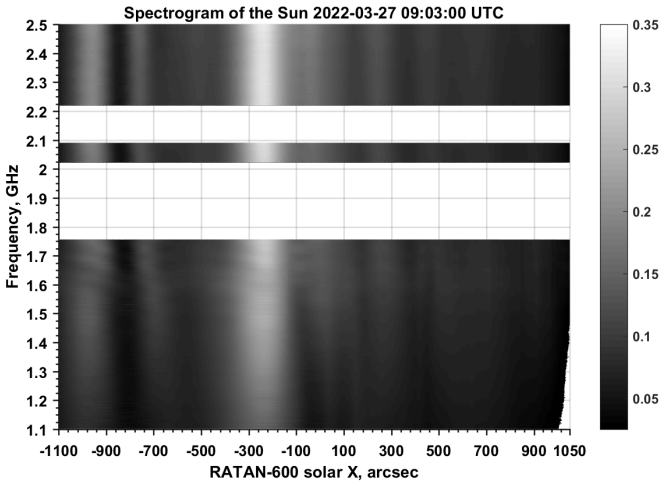

Figure 3: The resulting spectrogram, deconvolved with horizontal BP of the antenna system

1665, 1667 and 1720 MHz), equally shifted by 10 MHz. The frequency shift of all three lines then changes equally along the loop by 30 MHz, supposedly due to a change in the magnetic field magnitude. The second absorption band, observed above AR NOAA 2975, was a bit wider and the frequencies of the lines also shifted synchronously following the loop height change.

2. Solar radio emission in 3-18 GHz range observations with the RATAN-600

The radio emission of the quiet Sun and all the radio sources in different ARs form a superposition that we observe in each individual measurement. A PARAFAC model of a three-way array is given by three loading matrices: a matrix of the source positions; a matrix of their spectra, and a matrix of their amplitudes, or contributions in each measurement. We restore sequentially the radio emission of all groups of sources corresponding for each AR at each moment of observation.

Consider the radio emission of ARs NOAA 12996 and 12995 before and during the M1.2 flare, which occurred on 2022.04.29 at 07:30 UTC in 2996 (Fig. 4) over the AR polarity inversion line (PIL); the SDO/AIA image is rotated to match the RATAN-600 positional angle. There were no essential changes in the radio emission from ARs 2996 and 2995 within the period from 24.04 to 27.04; the radio images and spectrograms of these two ARs are presented in Fig. 5. The day before the flare occurred, the radio image of the AR 2996 changed dramatically due to the appearance of twisted loops, that manifested itself in the appearance of a group of sources that were closely located, but had spectral flux density maxima at different frequencies (Fig. 6). This was accompanied by the increase in the flux density in the range of 5–10 GHz, with the maximum spectral flux density at 6 GHz. We attribute this to a contribution of the gyrosynchrotron radio sources in the twisted magnetic tube [6]. The evolution of radio sources of AR 2995 during the observations was insignificant, while in the AR 2996 the form of the flux spectra changed during April 28–29, and new sources appeared before and during the flare. The flux spectra of the two radio sources above AR 2996 are presented in Fig. 7: the first one existed for the entire time of

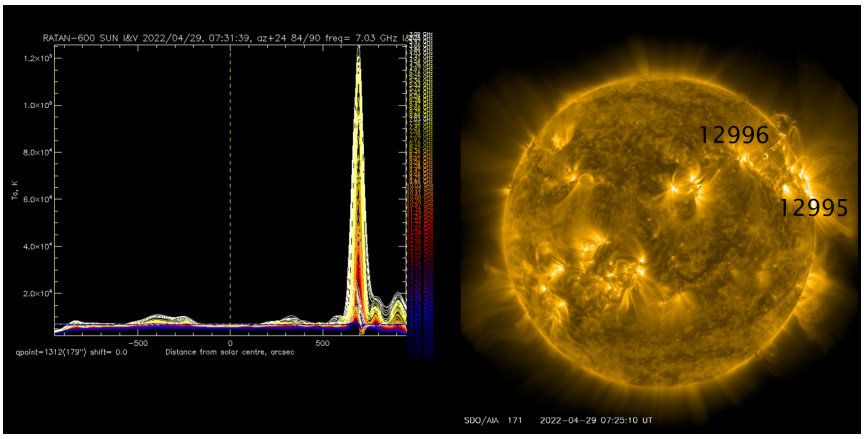

Figure 4: M1.2 N26W39 (2996) on 29.04.2022: *left*–data from RATAN-600 Solar complex; *right*—SDO/AIA UV image (171 Å)

observations, and the second one arose during the flare. Blue and red lines correspond to right and left circular polarization.

The SDO/AIA UV image from 2022.04.27 at 07:30:10 UTC reveals the double arc on the PIL of the AR 2996 (see Fig. 8). So, we can assume that the mechanism of double arc instability (DAI) [7] might drive this flare. In this case, the magnetic twist is also responsible for the flaring.

Conclusion

Using multivariate statistical analysis methods allows us differentiate the radio sources in the active regions on the Sun by their individual flux spectra and to analyze their evolution during the whole time they have been in sight, as well as reveal fine spectral effects and fast processes. We can even detect twisted magnetic loops in flare-productive ARs.

In the data from the latest measurements with the digital spectropolarimetric complex with RFI excision in the decimeter wavelength range with the RATAN-600 we detected an absorption line close to 1.6 GHz over the flare-productive ARs that may be attributed to the presence of hydroxyl molecule in cool coronal mass, such as solar prominences and coronal rain.

Acknowledgments

Observations with the SAO RAS telescopes are supported by the Ministry of Science and Higher Education of the Russian Federation. The renovation of telescope equipment is currently provided within the national project “Science and Universities”. The work was performed as part of the SAO RAS government contract approved by the Ministry of Science and Higher Education of the Russian Federation.

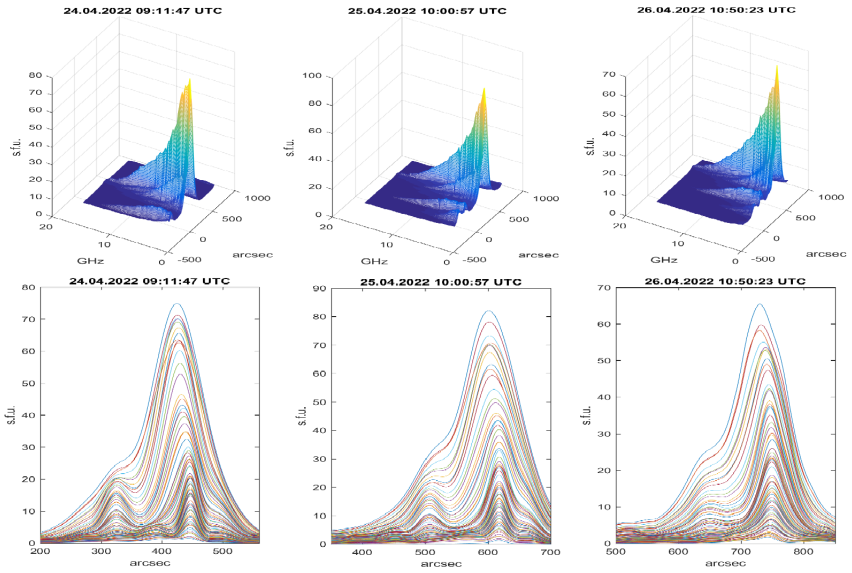

Figure 5: Radio emission on April 24–26, 2022 from ARs 2996 and 2995: *upper panel*—spectrogram; *lower panel*—radio image

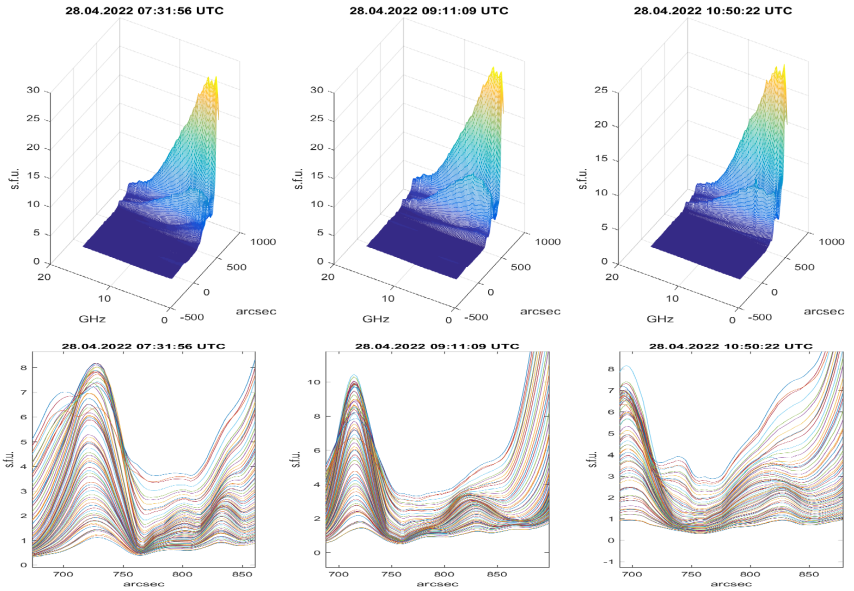

Figure 6: Radio emission on April 28, 2022 from ARs 2996 and 2995: *upper panel*—spectrogram; *lower panel*—radio image

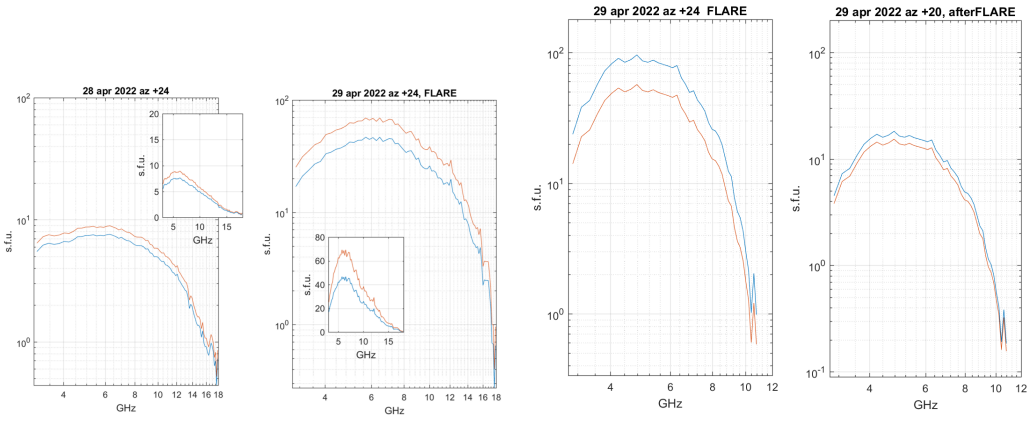

Figure 7: Evolution of the flux spectra of the radio sources on April 29–29, 2022 in ARs 2996

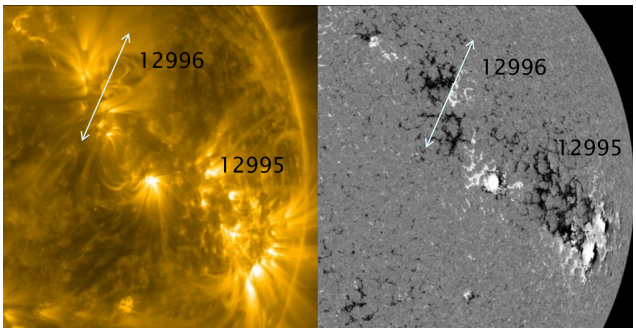

Figure 8: Double arc in the SDO image from 2022.04.27 at 07:30:10 UTC: *left*—AIA UV (171 Å); *right*—HMI image

References

[1] Sue Leurgans and Robert T. Ross, *Multilinear Models: Applications in Spectroscopy*, *Statist. Sci.* **7** (1992) 289

[2] Richard A. Harshman and Margaret E. Lundy, *PARAFAC: Parallel factor analysis*, *Computational Statistics & Data Analysis* **18** (1994) 39

[3] Rasmus Bro, *PARAFAC. Tutorial and applications*, *Chemometrics and Intelligent Laboratory Systems* **38** (1997) 149

[4] H. Zirin, B. M. Baumert, G. Hurford, *The microwave brightness temperature spectrum of the quiet sun*, *ApJ* **370** (1991) 779

[5] Kenji Maeda *et al.*, *Hyperfine structure of the hydroxyl free radical (OH) in electric and magnetic fields*, *New J. Phys.* **17** (2015) 045014

[6] I.N. Sharykin, A.A. Kuznetsov, *Modelling of Nonthermal Microwave Emission from Twisted Magnetic Loops*, *Sol Phys* **291** (2016) 1341

[7] Kusano *et al.*, *A physics-based method that can predict imminent large solar flares*, *ApJ* **843** (2017) 101